Journal of Power Sources 180 (2008) 695–703

Contents lists available at ScienceDirect

Journal of Power Sources

journal homepage: www.elsevier.com/locate/jpowsour

Characterization and performance of (La,Ba)(Co,Fe)O_3 cathode for solid oxide fuel cells with iron–chromium metallic interconnect

Yongda Zhen [a], San Ping Jiang [b,*]

[a] Institute of Chemical and Engineering Sciences, 1 Pesek Road, Jurong Island, Singapore 627833, Singapore
[b] School of Mechanical and Aerospace Engineering, Nanyang Technological University, 50 Nanyang Avenue, Singapore 639798, Singapore

ARTICLE INFO

Article history:
Received 21 November 2007
Received in revised form 21 January 2008
Accepted 19 February 2008
Available online 14 March 2008

Keywords:
Lanthanum cobalt ferrite-based perovskite cathode
Chromium-tolerant cathode
Chromium poisoning
Solid oxide fuel cell
Metallic interconnect
Oxygen reduction

ABSTRACT

$(La_{0.6}Ba_{0.4})(Co_{0.2}Fe_{0.8})O_3$ (LBCF) is synthesized by a sol–gel method as a Cr-tolerant cathode for intermediate-temperature solid oxide fuel cells (ITSOFCs). The electrochemical performance and Cr deposition process for the O_2 reduction reaction on LBCF cathodes in the presence and absence of a Fe–Cr alloy interconnect are investigated in detail, in comparison with a (La,Sr)(Co,Fe)O_3 (LSCF) electrode. Cr deposition occurs for the O_2 reduction reaction on LBCF electrodes in the presence of Fe–Cr alloy. Very different from that observed for the reaction on the LSCF cathode, Cr deposition on the LBCF electrode/gadolinia-doped ceria (GDC) electrolyte system is very small and shows little poisoning effect for O_2 reduction on LBCF electrode. The results demonstrate that the LBCF electrode has a high resistance towards Cr deposition and high tolerance towards Cr poisoning.

1. Introduction

The solid oxide fuel cell (SOFC) is an environmentally friendly and most efficient power generation technology with very low greenhouse gas emission. Progress in the reduction of the operating temperature of SOFCs enables the use of metals, especially chromia-forming ferrite stainless steels, as the interconnect owing to their high thermal and electronic conductivity, negligible ionic conductivity, good machineability, and low material cost [1]. Nevertheless, the application of these chromia-forming alloys as interconnects still poses many challenges, even at reduced temperatures. The oxide scale formed on the surface of the alloys after exposure in the SOFC environment results in high electrical resistance and causes degradation of stack performance [2–4]. Furthermore, under high temperature, volatile Cr species such as CrO_3 and $CrO_2(OH)_2$ are generated over the oxide scale in oxidizing atmospheres [5,6]. The gaseous Cr species can cause rapid deterioration of the performance of SOFCs due to the poisoning of cathodes such as (La,Sr)MnO_3 (LSM) and (La,Sr)(Co,Fe)O_3 (LSCF) for the O_2 reduction reaction [7–15].

The effect of Cr poisoning can be reduced by optimization of the composition and microstructure of the Fe–Cr alloy and by the development of conductive and dense protective coatings on the alloy to reduce the volatility of Cr species [2,16]. Recently, we have proposed a strategy to identify and develop Cr-deposition resistant and tolerant cathode for SOFCs [17,18]. The strategy is based on a theory that Cr deposition under SOFC operating conditions is dominated by a chemical dissociation reaction, which is initiated by a nucleation reaction between the gaseous Cr species and nucleation agents, such as manganese species (Mn^{2+}) generated under cathodic polarization in a LSM electrode/zirconia electrolyte system or SrO species enriched originally at the electrode surface in the LSCF electrode/ceria electrolyte system [10,12]. The chemical nature of the Cr deposition process implies that it is possible to develop cathode material with high resistance towards Cr deposition by proper design and modification of the cathode composition. The strategy appears to be supported by the results of the interaction between a La(Ni,Fe)O_3 (LNF) cathode and a Fe–Cr alloy interconnect [17,19]. Different to that on the LSM and LSCF cathodes, there is no visible Cr deposition at the LNF cathode|YSZ electrolyte interface or on the LNF surface. This indicates that the deposition of Cr species is significantly inhibited on the LNF cathode and this is most likely due to the absence of nucleation agents, such as Mn and SrO species, in LNF materials.

On the other hand, the lanthanum cobalt ferrite-based perovskites have been widely investigated as the possible cathodes for intermediate-temperature SOFCs (ITSOFCs) due to their high mixed electronic and ionic conductivities [20–25]. For example,

* Corresponding author. Fax: +65 6791 1859.
E-mail address: mspjiang@ntu.edu.sg (S.P. Jiang).

0378-7753/$ – see front matter © 2008 Elsevier B.V. All rights reserved.
doi:10.1016/j.jpowsour.2008.02.093

both LSCF [22] and $(Sm_{0.5}Sr_{0.5})CoO_3$ (SSC) [24] exhibit satisfactory electrochemical performance for oxygen reduction at intermediate temperatures of 600–800 °C. Most recently, $(Ba_{0.5}Sr_{0.5})(Co_{0.8}Fe_{0.2})O_3$ (BSCF) oxide has been found to exhibit excellent activity as a new cathode material [25]. Thus, replacing Sr with Ba in LSCF would reduce the Cr deposition according to the proposed strategy [17,18] and at the same time maintain high electrocatalytic activity for O_2 reduction reaction. This study involves the development and characterization of Sr-free $(La,Ba)(Co,Fe)O_3$ as a high performance cathode with high Cr-deposition resistance and Cr-tolerance for ITSOFCs. A comparative study of LBCF and LSCF cathodes for O_2 reduction in the presence of a Fe–Cr alloy interconnect indicates that LBCF is a promising Cr-tolerant cathode for ITSOFCs with metallic interconnects.

2. Experimental

Gadolinia-doped ceria ($Gd_{0.2}Ce_{0.8}O_2$, GDC) electrolyte discs were prepared by solid-state reaction synthesis from high-purity CeO_2 (99%, Praxair Specialty Ceramics, USA) and Gd_2O_3 (99%, Praxair Specialty Ceramics, USA). The mixed oxides were ball milled in ethanol with yttria-stabilized zirconia medium for 20 h. After drying, the mixture was pressed into discs and sintered at 1600 °C for 6 h in air. The sintered electrolyte thickness and diameter were about 1 and 21 mm, respectively.

$(La_{0.6}Ba_{0.4})(Co_{0.2}Fe_{0.8})O_3$ powder was synthesized by the Pechini method [26]. The chemicals, $La(NO_3)_3{\cdot}6H_2O$, $Ba(NO_3)_2$, $Co(NO_3)_3{\cdot}6H_2O$, $Fe(NO_3)_3{\cdot}9H_2O$, citric acid and ethylene glycol were obtained from Sigma–Aldrich. Stoichiometric amounts of $La(NO_3)_3{\cdot}6H_2O$, $Ba(NO_3)_2$, $Co(NO_3)_2{\cdot}6H_2O$, $Fe(NO_3)_3{\cdot}9H_2O$ were dissolved in de-ionized water under mild stirring. Then, appropriate amounts of citric acid and ethylene glycol were introduced into the solution with a molar ratio of citric acid to total cations of 3:1. The resulting solution was stirred for 1 h at room temperature and then heated at 100 °C on a hotplate until a dark resin was formed. After being baked at 180 °C for overnight in an oven, the obtained resin was then calcined in air at 950 °C for 5 h to obtain the final LBCF powder. The phase of the LBCF powder was examined by X-ray diffraction (XRD). For the purpose of comparison, $(La_{0.6}Sr_{0.4})(Co_{0.2}Fe_{0.8})O_3$ (LSCF) powder (99.9%, Nextech, USA) was also used.

The cathode ink was prepared by mixing LBCF or LSCF powder with polyethylene glycol. The ink was then applied to a GDC electrolyte by screen-printing method, followed by sintering at 1000 °C for 2 h in air. The electrode thickness was ~30 μm and the electrode area was 0.5 cm^2. Platinum paste (Ferro Corporation, USA) was painted on the other side of the GDC electrolyte substrate to serve as the counter and reference electrodes. The counter electrode was symmetrical to the working electrode and the reference electrode was painted as a ring around the counted electrode. The gap between the counter and reference electrodes was ~4 mm. The Pt electrodes were sintered at 950 °C for 1 h in air.

Fe–Cr alloy (RA446 with 23–27 wt% Cr, 1.5% Mn, 1% Si, 0.2% C, 0.12% N and the remainder Fe; Rolled Alloy Co., Canada) was used as the interconnect. The alloys were machined into coupons (12 mm × 12 mm × 4 mm) with channels (1.2 mm × 1.2 mm) cut on one side of the coupon. Air was directed to the channels through an alumina tube. Two Pt wires were spot-welded to the alloy to serve as voltage and current probes, respectively. The interconnect was placed directly on the LBCF electrode coating. In this arrangement, the alloy also acted as a current-collector. Air (Industrial grade, H_2O content <3 ppm), after drying through a molecular sieve, was used. The flow rate of the air was 100 ml min^{-1}. The cell configuration and the arrangement of the Fe–Cr alloy interconnect have been reported in previous publications [11,14].

The initial electrochemical behaviour of LBCF and LSCF electrodes was evaluated under a constant-current density of 200 mA cm^{-2} in air at 900 and 800 °C. The polarization potential ($E_{cathode}$) was measured against the Pt|air reference electrode. The current passage was interrupted from time to time to undertake electrochemical impedance spectroscopy (EIS) measurements. A Solartron 1260 frequency response analyzer in combination with a 1287 electrochemical interface was used for EIS measurements, over a frequency range of 100 kHz to 0.1 Hz and with a signal amplitude of 10 mV. EIS measurements were made at open-circuit. The electrode ohmic resistance (R_Ω) was determined from the high frequency intercept and the electrode interface (polarization) resistance (R_E) was obtained from the difference between the high- and low-frequency intercepts on the impedance spectrum. The overpotential (η) can be obtained from $E_{cathode}$ and R_Ω; i.e.

$$\eta = E_{cathode} - jR_\Omega \quad (1)$$

where j is the current density and R_Ω is the electrode ohmic resistance.

Scanning electron microscopy (SEM, JEOL 6360, Japan) and X-ray energy dispersion spectroscopy (EDS, Oxford, UK) were used to examine the electrode morphology and the element distribution. In order to view the GDC electrolyte surface in contact with the electrode, the electrode coating was removed by treatment with 20% HCl acid and then washing in de-ionized water. The electrochemical performance and Cr-deposition for O_2 reduction on the LSCF cathode has been reported in Ref. [10].

3. Results and discussion

3.1. Performance and characteristics in presence of Fe–Cr alloy at 900 °C

X-ray diffraction (XRD) patterns of LBCF and LSCF powders are given in Fig. 1. All the major XRD patterns belong to the perovskite structure, which indicates the formation of a single perovskite phase of the LBCF and LSCF powders.

The initial impedance responses and polarization behaviour of a LBCF electrode for O_2 reduction were studied under a cathodic current of 200 mA cm^{-2} at 900 °C in the absence of a Fe–Cr alloy interconnect, as shown in Fig. 2. The impedance responses measured at open-circuit are quite small, which demonstrates the high electrochemical activity of the LBCF electrode for O_2 reduction. The initial electrode polarization resistance (R_E) is ~0.04 Ω cm^2

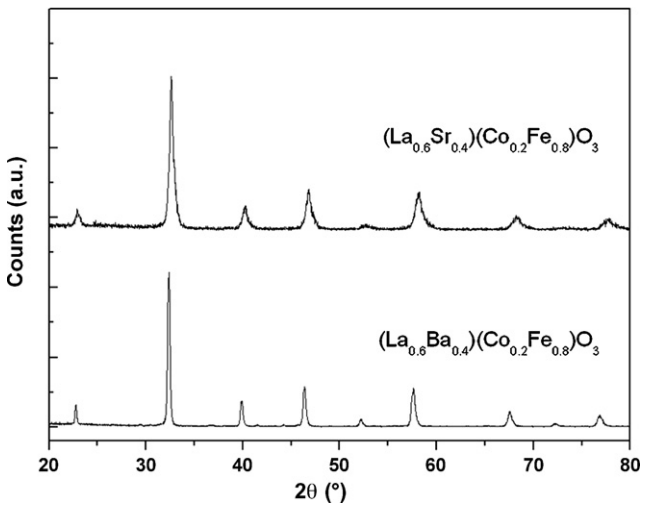

Fig. 1. XRD patterns of LBCF and LSCF powders.

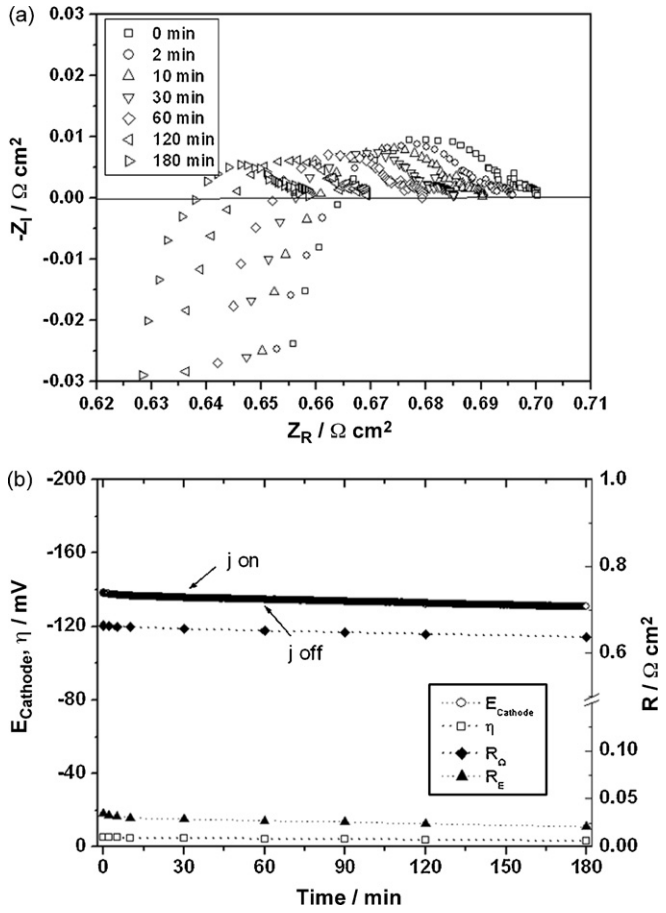

Fig. 2. Initial (a) impedance and (b) polarization curves of LBCF electrode as function of current passage time of 200 mA cm^{-2} in absence of Fe–Cr alloy interconnect at 900 °C.

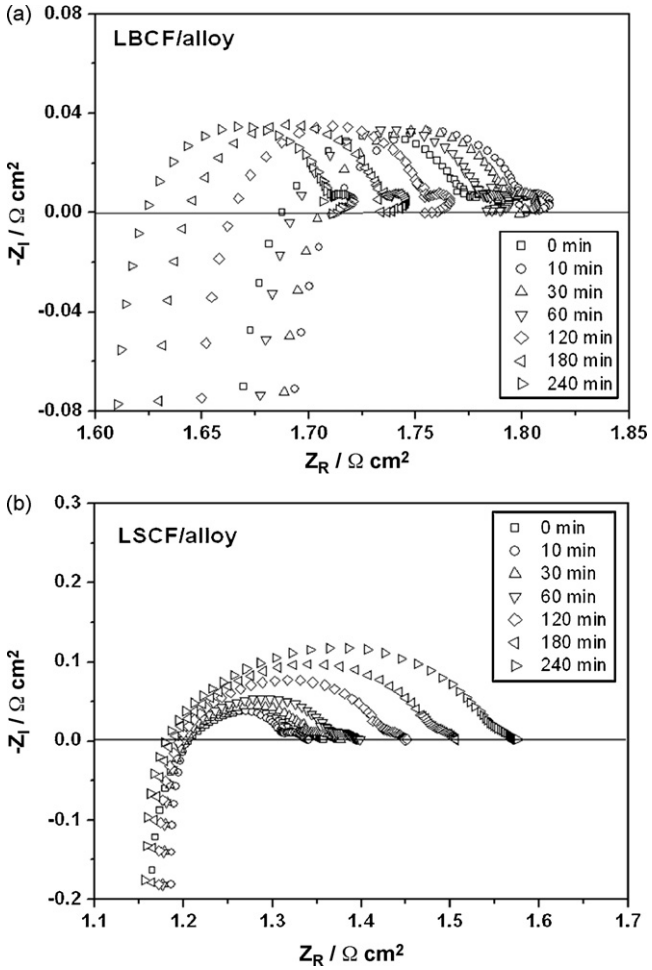

Fig. 3. Initial impedance responses of LBCF and LSCF electrodes as function of current passage time of 200 mA cm^{-2} in the presence of Fe–Cr alloy interconnect at 900 °C.

and remains more or less unchanged with the passage of current (Fig. 2a). The small reduction in ohmic resistance (R_Ω) is most likely due to an improved contact between the electrode and the electrolyte. The high activity of LBCF electrode is also indicated by a low overpotential (η is ~6 mV at 200 mA cm^{-2}), as shown in Fig. 2b. The potential of the cathode ($E_{cathode}$) changes very little with passage of current. This shows that cathodic polarization has little effect on the electrocatalytic activity of the LBCF electrode, similar to that for the LSCF electrode [27]. The very low polarization resistance and overpotential for O_2 reduction show that LBCF is a promising cathode material for ITSOFCs.

Fig. 3 shows the initial impedance responses of LBCF and LSCF electrodes for oxygen reduction at 200 mA cm^{-2} and 900 °C in the presence of a Fe–Cr alloy interconnect. For the LSCF electrode, the impedance arcs increase significantly with cathodic polarization. The initial R_E is 0.13 Ω cm^2 and increases to 0.43 Ω cm^2 after 240 min of current passage. The significant increase in R_E shows a rapid degradation in the electrochemical activity of the LSCF for oxygen reduction due to the significant poisoning effect of Cr species [10]. In the case of the LBCF electrode, there is essentially no change in the impedance arc with cathodic polarization (Fig. 3a). The initial R_E is 0.10 Ω cm^2 and after a current passage for 240 min, the value is 0.09 Ω cm^2, i.e., almost the same as the initial R_E.

Fig. 4 presents the initial polarization behaviour of LBCF and LSCF electrodes for oxygen reduction as a function of the passage of current at 200 mA cm^{-2} and 900 °C in the presence of a Fe–Cr alloy interconnect. Very different to that in the absence of a Fe–Cr alloy interconnect, the polarization potential ($E_{cathode}$) increases rapidly with current passage and reached a potential region where the increase in $E_{cathode}$ is much slower for the reaction on LBCF in the presence of a Fe–Cr alloy interconnect (Fig. 4a). Similar polarization behaviour is also observed for oxygen reduction on the LSCF electrode in the presence of Fe–Cr alloy (Fig. 4b). The very different $E_{cathode}$ behaviour with the current for oxygen reduction in the absence and presence of Fe–Cr alloy is a clear indication of the significant poisoning effect of the gaseous Cr species, especially on the surface processes such as the dissociation adsorption and diffusion of oxygen for the reaction at the cathodes [11,27]. The increase in the polarization is mainly due to the increase in overpotential (η) according to Eq. (1), as the change in the electrode ohmic resistance (R_Ω) is negligible with the current passage time.

The polarization behaviour and the change in η and R_E as a function of current passage time for O_2 reduction on the LBCF and LSCF electrodes in the presence of Fe–Cr alloy interconnect for 20 h at 900 °C are shown in Fig. 5. In the case of the LSCF electrode, $E_{cathode}$ increased monotonically with time (Fig. 5b). The initial η is 21 mV and there is a significant increased to 343 mV after 20 h. R_E also increases from 0.21 to 0.79 Ω cm^2 during the same interval. The marked increase in η and R_E shows the significant poisoning effect of gaseous Cr species and solid Cr deposits on oxygen reduction at the LSCF electrode [10]. For oxygen reduction on the LBCF electrode, however, the increase in $E_{cathode}$ is much slower. $E_{cathode}$ increases initially but stabilizes after about 200 min. The initial η is about 16 mV and rises to 95 mV after 180 min. At the end of 20 h, η is

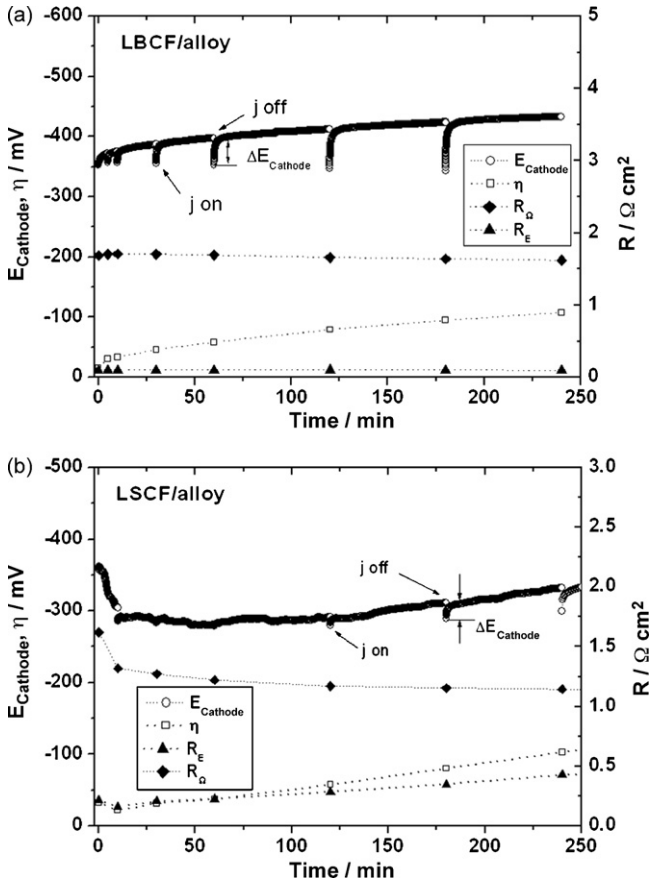

Fig. 4. Initial polarization curves of LBCF and LSCF electrodes as function of current passage time of 200 mA cm^{-2} in presence of Fe–Cr alloy interconnect at 900 °C.

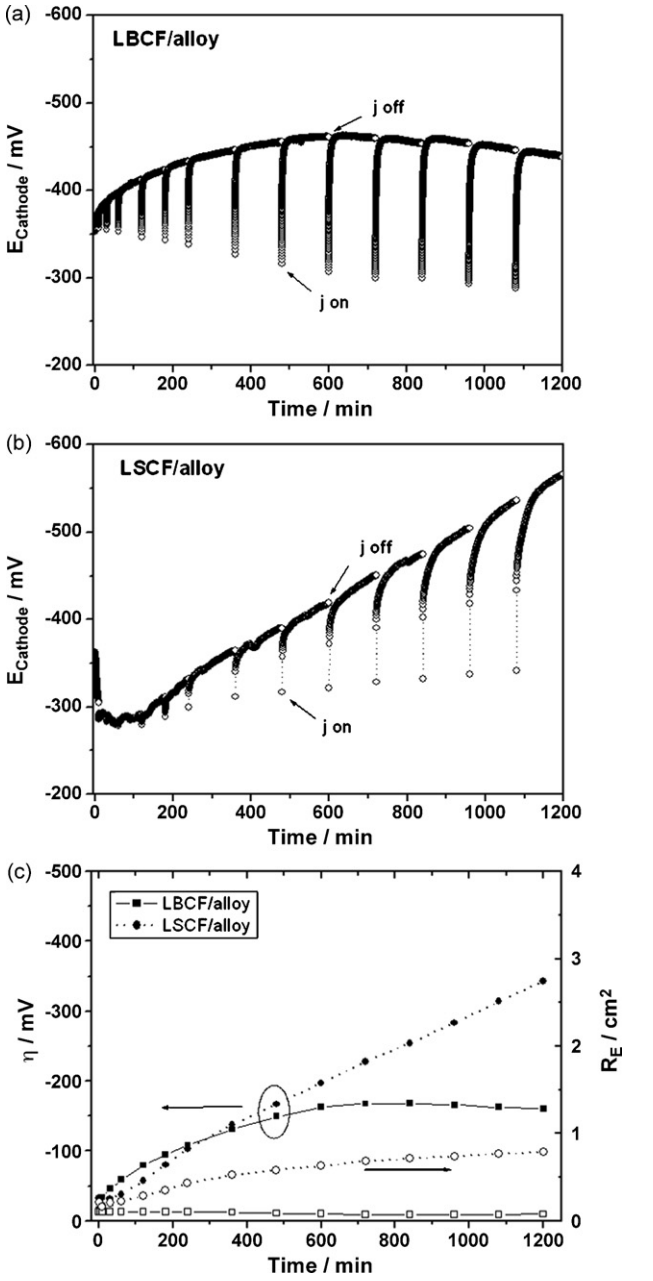

Fig. 5. Polarization behaviours as function of current passage time for O_2 reduction on LBCF and LSCF electrodes in presence of Fe–Cr alloy interconnect at 200 mA cm^{-2} and 900 °C for 20 h. Corresponding change of overpotential (η) and polarization resistance (R_E) for O_2 reduction is shown in (c). The impedance is measured at open-circuit.

160 mV. Most importantly, the polarization resistance of LBCF for oxygen reduction is stable with current passage. R_E is 0.08 Ω cm^2 after 20 h, similar to the initial value of 0.10 Ω cm^2. This indicates that LBCF has a high tolerance towards Cr species.

Fig. 6 presents SEM micrographs of the surface and cross-sections of the LBCF and LSCF cathodes after current passage at 200 mA cm^{-2} and 900 °C in the presence of a Fe–Cr alloy interconnect for 20 h. For the purpose of comparison, SEM micrographs of the freshly prepared LBCF and LSCF are also shown in Fig. 6(e) and (f). The corresponding EDS analysis is given in Fig. 7. The electrode surface shown is located under the rib of the interconnect. Significant deposition of Cr species is observed on the LSCF electrode surface such that it is almost completely covered by large deposited particles (Fig. 6(b)). Fine LSCF particles (less than 0.1 μm) are almost invisible. The Cr deposits on the LSCF electrode surface are identified as a $SrCrO_4$ phase [10]. The significant deposition of Cr species is also indicated by the EDS results (Fig. 7b). The deposition of Cr species occurs preferentially on the surface of the LSCF electrode and there are some isolated Cr deposits inside the electrode coating (Fig. 6(d)). Such a deposition pattern of Cr species on the LSCF electrode has also been reported by others [15,28]. By contrast, there is no visible deposition of large Cr crystals/deposits on the LBCF electrode surface. After the current passage at 900 °C for 20 h in the presence of Fe–Cr alloy interconnect, the microstructure of the LBCF electrode is characterized by fine and uniformly distributed particles (≤~0.5 μm) with fine pores Fig. 6(a) and (c), i.e., similar to that of freshly prepared LBCF (Fig. 6(e)). On the other hand, a comparative analysis of the EDS results of the LBCF coating shows the deposition of Cr species (Fig. 7(a) and (c)). For pure LBCF without Cr contamination, the $La_{L\alpha}/La_{L\beta}$ atomic ratio is 3.80 (Fig. 7(c)). After polarization in the presence of a Fe–Cr alloy for 20 h, the $La_{L\alpha}/La_{L\beta}$ atomic ratio decreases substantially to 1.24 (Fig. 7(a)). This is due to the fact that the Kα X-ray peak of Cr overlaps with the Lβ peak for La. The EDS pattern also shows an increasing intensity of Ba in comparison with that of the pure LBCF coating. The $Ba_{L\alpha}/La_{L\alpha}$ ratio increases from 0.69 to 1.08. This indicates that deposition of Cr species on the LBCF electrode surface may be induced by BaO segregated on the LBCF electrode surface. The intensity of Cr at the LBCF electrode, however, is much smaller than at the LSCF electrode, which indicates that the deposition reaction of Cr species at the former electrode is kinetically slow.

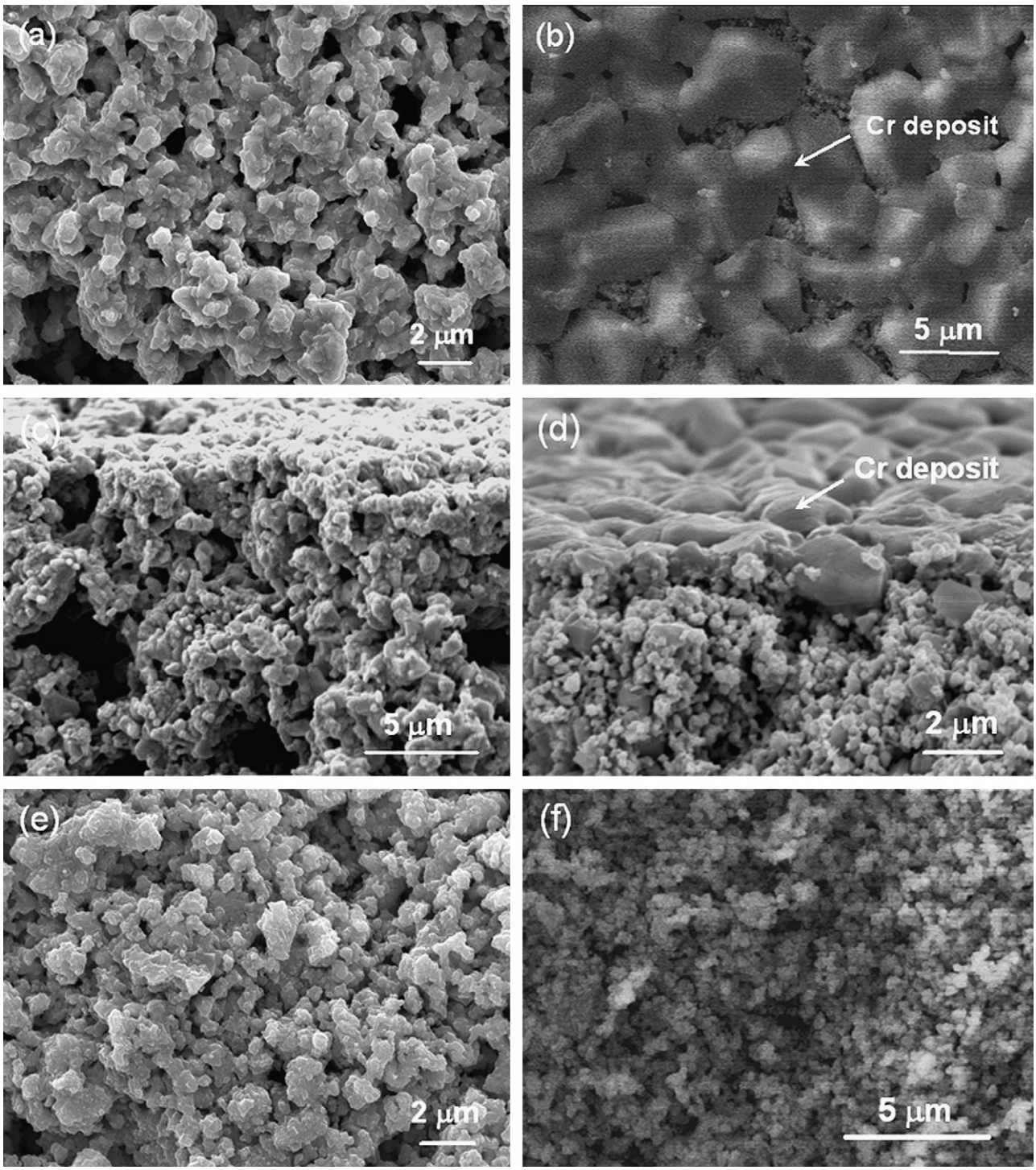

Fig. 6. SEM micrographs of surface and cross-section of (a) and (c) LBCF, and (b) and (d) LSCF electrodes after current passage at 200 mA cm^{-2} and 900 °C for 20 h in air in presence of Fe–Cr alloy interconnect. SEM micrographs of freshly prepared LBCF and LSCF electrode surface are shown in (e) and (f), respectively.

3.2. Performance and characteristics in presence of Fe–Cr alloy at 800 °C

The electrochemical activity for oxygen reduction and the characteristics of Cr deposition on LBCF electrodes were also investigated at 800 °C in the presence of a Fe–Cr alloy interconnect. Fig. 8 shows the electrochemical performance of a LBCF electrode for oxygen reduction at 200 mA cm^{-2} and 800 °C in the presence of a Fe–Cr alloy interconnect. The exact reason for the increase in R_Ω is not clear at this stage. One possibility for the increase in the electrode ohmic resistance at 800 °C in comparison with that at 900 °C (Fig. 3) could be related to the greater resistance of the oxide scale at lower temperature. Both polarization resistance and overpotential are very stable for the reaction at 800 °C. After current passage for 20 h, R_E is 0.11 Ω cm^2, i.e., almost the same as the initial R_E value of 0.13 Ω cm^2. The overpotential at 200 mA cm^{-2} varies between 13 and 15 mV and there is basically no change in the value (Fig. 8(b)). The impedance and polarization behaviour are similar to

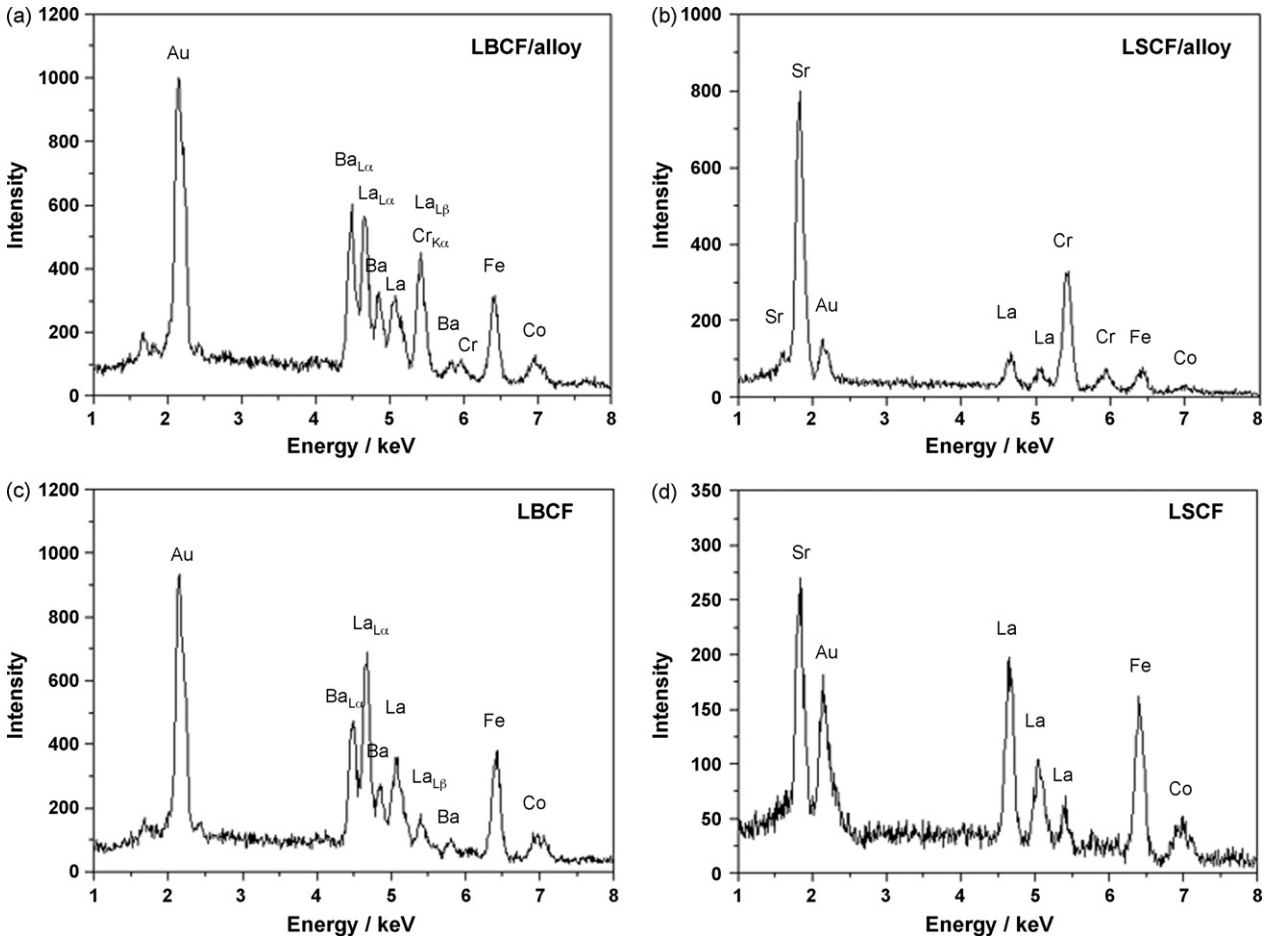

Fig. 7. EDS patterns of (a) LBCF electrode surface (shown in Fig. 6(a) and (b) LSCF electrode surface (shown in Fig. 6b) after current passage at 200 mA cm^{-2} and 900 °C for 20 h in presence of Fe–Cr alloy interconnect. EDS patterns of freshly prepared LBCF and LSCF electrode coatings are shown in (c) and (d), respectively.

the reaction in the absence of a Fe–Cr alloy interconnect. The very stable electrochemical performance for oxygen reduction at 800 °C shows that the poisoning effect of gaseous Cr species is nearly negligible.

Fig. 9 shows SEM images and corresponding EDS patterns for a LBCF electrode surface after a current passage of 200 mA cm^{-2} at 800 °C for 20 h in the presence of a Fe–Cr alloy interconnect. The contact areas between the interconnect and the electrode coating can be easily identified in the backscattered electron micrograph, as shown in Fig. 9(c). The microstructure and morphology of the LBCF electrode coating under the channel and the rib of the metallic interconnect are identical (Fig. 9(a) and (b)). As at 900 °C, there is no visible change in the microstructure of the LBCF electrode coating after being polarized at 800 °C in the presence of Fe–Cr alloy, compared with that of the freshly prepared LBCF electrode (Fig. 6(e)). For the LBCF electrode coating under the rib of the Fe–Cr

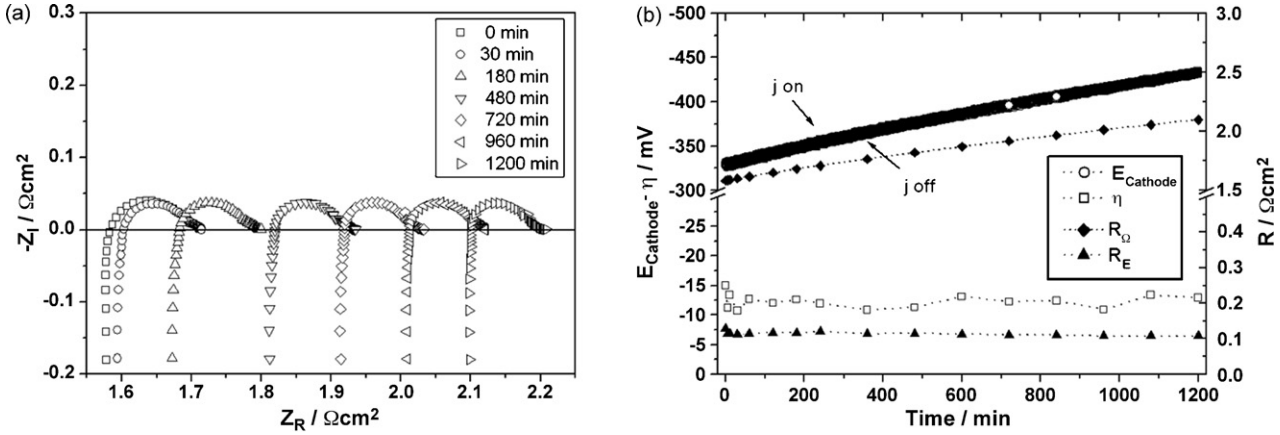

Fig. 8. Initial (a) impedance and (b) polarization curves of LBCF electrode as function of passage time of 200 mA cm^{-2} in presence of Fe–Cr alloy interconnect at 800 °C for 20 h.

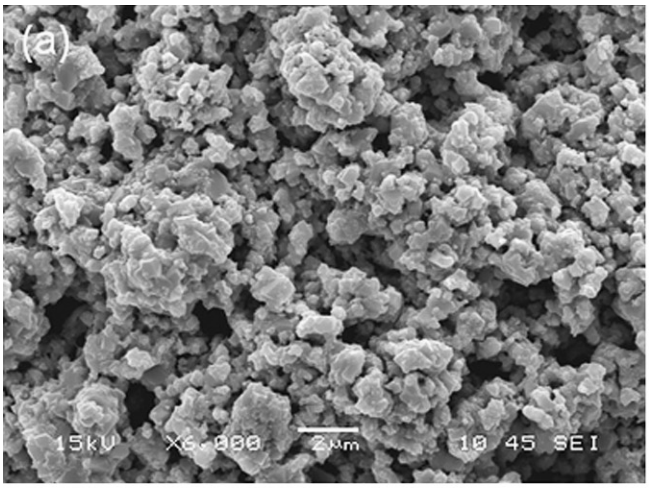

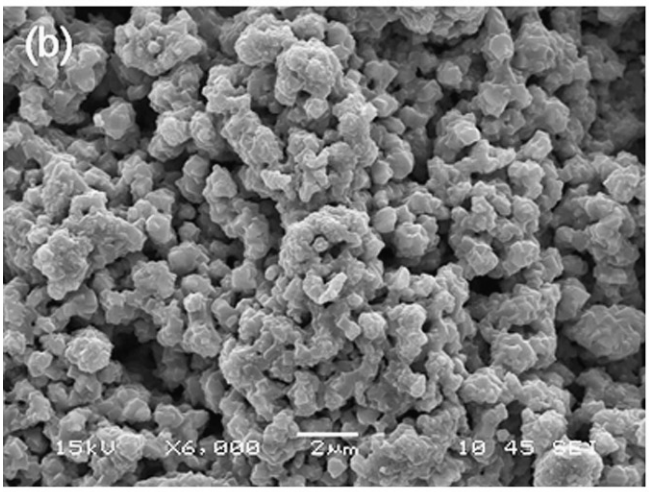

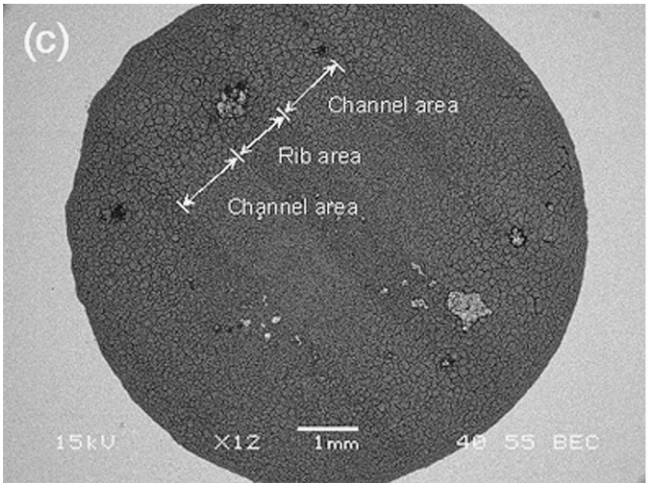

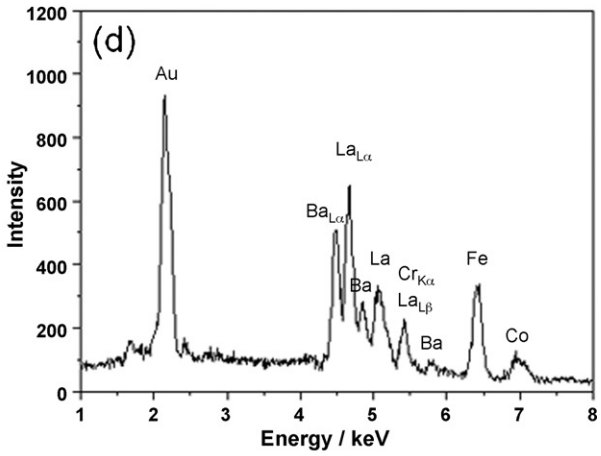

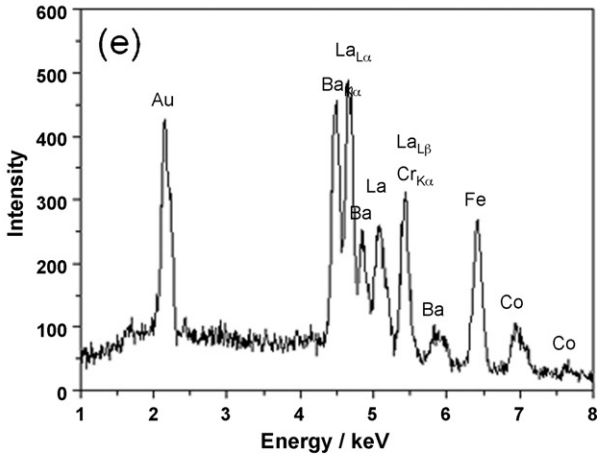

Fig. 9. SEM micrographs and EDS patterns of LBCF electrode after current passage at 200 mA cm^{-2} and 800 °C in presence of Fe–Cr alloy interconnect for 20 h: (a) electrode surface under channel of interconnect, (b) electrode surface under rib of interconnect, (c) overview showing the contact marker of channel and rib areas of interconnect, (d) EDS pattern of electrode coating under channel of Fe–Cr alloy interconnect, and (e) EDS pattern of electrode under rib of interconnect.

alloy interconnect, the $La_{L\alpha}/La_{L\beta}$ atomic ratio is 1.57 (Fig. 9(e)), which is significantly smaller than 3.25 observed for the coating under the channel of the interconnect (Fig. 9(d)). This indicates that the Cr deposition on the LBCF surface is in direct contact with the Fe–Cr alloy interconnect. Nevertheless, the deposition of Cr species under the rib of interconnect species is still very low, as indicated by the fact that there is no significant difference in the electrode microstructure under the rib or channel of the interconnect. The different intensity of Cr under the channel and rib of the interconnect shows the deposition of Cr species is related to the flow field of the interconnect, similar to Cr deposition in the LSM/YSZ [13] and LSCF/GDC systems [10].

Fig. 10 presents SEM images and corresponding EDS patterns of a LBCF electrode after current passage at 200 mA cm^{-2} and 800 °C

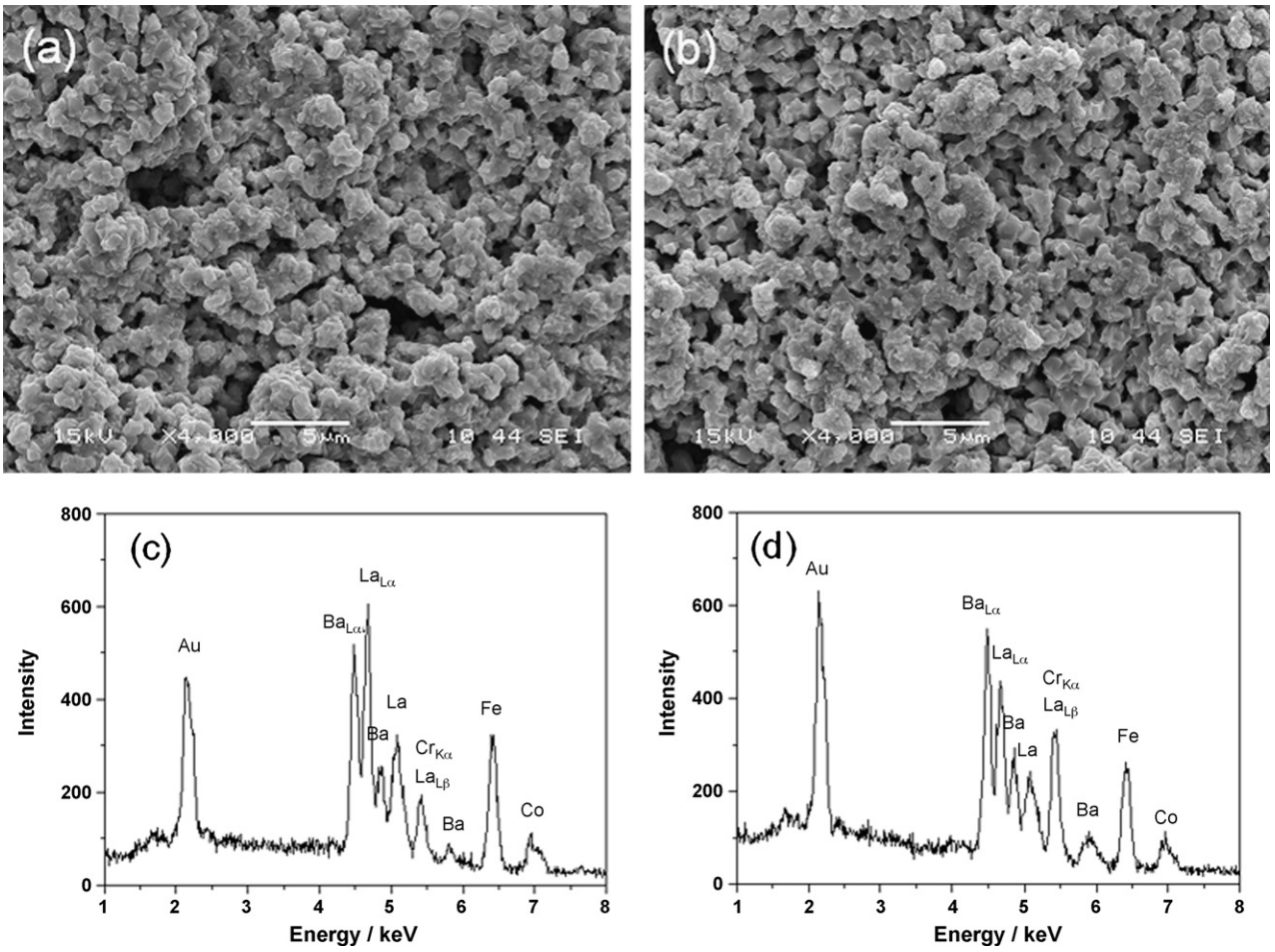

Fig. 10. SEM micrographs and EDS patterns of LBCF electrode after current passage at 200 mA cm^{-2} and 800 °C in the presence of Fe–Cr alloy interconnect for 60 h: (a) and (c) SEM and EDS of electrode surface under channel of interconnect, and (b) and (d) SEM and EDS of electrode surface under rib of interconnect.

for 60 h in the presence of a Fe–Cr alloy interconnect. Even after 60 h, there is no obvious change in the microstructure of the LBCF as compared with that of the freshly prepared LBCF electrode. Fine particles and the well-distributed pores are clearly observed. Nevertheless, the intensity of Cr on the LBCF electrode coating under the channel of the interconnect ($La_{L\alpha}/La_{L\beta}$ ratio = 3.13) is much smaller than that ($La_{L\alpha}/La_{L\beta}$ ratio = 1.33) under the rib. In addition, for the LBCF electrode coating under the rib of the interconnect, EDS analysis shows a much higher intensity of Ba and Cr as compared with that with La, Co and Fe. The $Ba_{L\alpha}/La_{L\alpha}$ ratio is 1.26, i.e., much higher than 0.69 of the freshly prepared LBCF material. This again indicates that the deposition of Cr species on the LBCF electrode is associated with Ba species on the surface.

Fig. 11 presents a SEM image and EDS pattern of the GDC electrolyte surface in contact with a LBCF electrode in the presence of a Fe–Cr alloy after current passage at 200 mA cm^{-2} and 800 °C for 60 h. The LBCF electrode coating was removed by HCl acid treatment. In a separate experiment, it was found that chromium oxide and chromium deposits do not dissolve in the dilute HCl solution used in the present study. The electrolyte surface is clean without any Cr deposition. The fine concave marks are the contacts between the LBCF particles and GDC electrolyte, formed during sintering of the electrode. EDS analysis shows a typical pattern of a GDC material (Fig. 11(b)), which indicates no other phases in the GDC electrolyte. This is similar to that on the LSCF electrode, showing again that Cr does not deposit preferentially at the LBCF electrode|GDC electrolyte interface.

3.3. Cr deposition at LBCF electrode

As shown in earlier studies [10,14], the interaction between the Fe–Cr alloy interconnect and the (La,Sr)(Co,Fe)O_3 electrode leads to preferential and significant deposition of Cr species on the surface of LSCF electrode, forming $SrCrO_4$ crystals with a scheelite structure. The nucleation and grain growth of the Cr deposition process at the LSCF electrodes is most likely controlled by the interaction between gaseous Cr species (e.g., CrO_3) and SrO species initially existed or segregated on the LSCF electrode surface under the polarization conditions [10,14]. The deposition of large Cr crystals on the electrode surface and inside the electrode bulk blocks the oxygen diffusion and transportation process, which results in a rapid degradation of the electrode performance for oxygen reduction. Such a poisoning effect of the solid Cr deposits is irreversible, as indicated by the rapid increase in η and R_E.

Chromium deposition also occurs on the LBCF electrode for oxygen reduction in the presence of a Fe–Cr alloy interconnect, as shown clearly in this study. In contrast to that observed on the LSCF electrode, the deposition of Cr species has little effect on the microstructure or morphology of the LBCF electrode. The increased Ba content on the LBCF electrode surface after polarization in the presence of Fe–Cr alloy indicates that barium plays an important role in Cr deposition. The ionic radius of Ba^{2+} is 1.61 Å, i.e., significantly larger than 1.16 Å of La^{3+} [29]. In the case of $LaCrO_3$, the solubility of Ba at the A-site is below 10 mol.% and high Ba doping leads to the formation of a second phase, $BaCr_2O_4$ [30]. In the

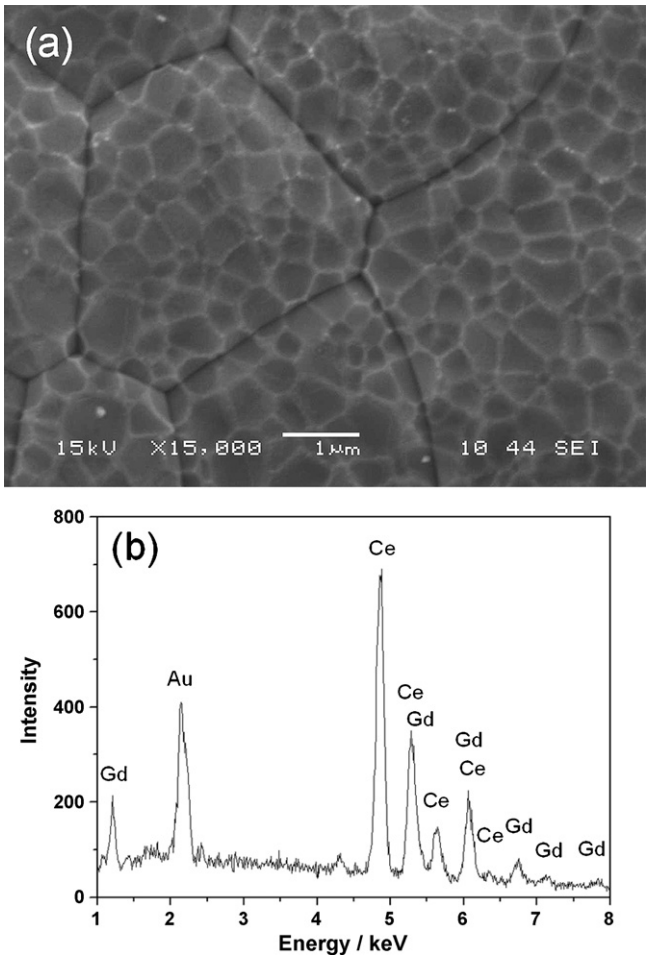

Fig. 11. SEM micrograph and EDS pattern of GDC electrolyte surface in contact with LBCF electrode in presence of Fe–Cr alloy interconnect after current passage at 200 mA cm^{-2} and 800 °C for 60 h. LBCF electrode coating removed by HCl acid treatment.

present study, a stoichiometric $(La_{0.6}Ba_{0.4})(Co_{0.2}Fe_{0.8})O_3$ composition is used. Thus, in stoichiometric LBCF, segregation of BaO could occur, particularly for high Ba doping level. The nucleation reaction could occur between gaseous Cr species such as CrO_3 and a nucleation agent, namely BaO segregated on the surface of LBCF electrodes, to form Cr–Ba–O nuclei. Thus, similar to the reaction mechanism of Cr deposition on LSCF electrodes [10,14], the deposition process on LBCF can be written as:

$$CrO_3 + BaO \rightarrow Cr\text{–}Ba\text{–}O(\text{nuclei}) \quad (2)$$

$$Cr\text{–}Ba\text{–}O(\text{nuclei}) + CrO_3 \rightarrow Cr_2O_3 \quad (3)$$

$$Cr\text{–}Ba\text{–}O(\text{nuclei}) + CrO_3 + BaO \rightarrow BaCr_2O_4 \quad (4)$$

The $BaCr_2O_4$ phase is not detected on the surface not the bulk of the LBCF cathode despite the increased barium content on the surface after polarization in the presence of a Fe–Cr alloy interconnect. The fact that their is no visible change in the microstructure on the surface or the inside the LBCF electrode indicates that formation of Cr_2O_3 and grain growth of a $BaCr_2O_4$ phase between gaseous Cr species and Cr–Ba–O nuclei is kinetically a very slow process. The exact reaction steps and the phase formation of the Cr deposits in the case of LBCF electrodes require further study.

The most important finding of the present study is the high electrochemical activity and stability of LBCF electrodes for oxygen reduction despite the observed Cr deposition at 900 and 800 °C. In comparison with the reaction on the LSCF electrode, η and R_E for oxygen reduction on the LBCF electrode are both much lower. The stable η and R_E values for the reaction at the LBCF electrode in the presence of Fe–Cr alloy interconnect also imply that the poisoning effect of Cr deposits on the reaction is very low or negligible under the conditions studied here. The results show that the LBCF electrodes have a high resistance towards Cr deposition and a high tolerance towards the Cr poisoning.

4. Conclusions

The characteristics and performance of stoichiometric LBCF electrode in the presence of a Fe–Cr alloy interconnect have been studied at 900 and 800 °C. As compared with the LSCF electrode, deposition of Cr species at the LBCF electrode is very low and has basically no detrimental effect on the microstructure of the electrode. Most interesting, LBCF electrode has a very high and stable electrochemical activity for oxygen reduction in the presence of a Fe–Cr alloy interconnect. The results demonstrate that the LBCF electrode has high resistance and tolerance towards the Cr deposition and poisoning. LBCF is a promising cathode material for intermediate-temperature SOFCs when a chromia-forming alloy interconnect is used.

Chromium deposition on LBCF is most likely dominated by the interaction between gaseous Cr species and Ba species (e.g., BaO) segregated on the LBCF surface, to form Cr–Ba–O nuclei. The low Cr deposition and no visible change in the electrode microstructure after polarization in the presence of Fe–Cr alloy indicates that the formation of solid Cr deposits such as Cr_2O_3 or $BaCr_2O_4$ could be kinetically a very slow process. Further studies are required to understand the Cr deposition process on LBCF electrodes under cathodic polarization conditions.

References

[1] J.W. Fergus, Mater. Sci. Eng. A 397 (2005) 271.
[2] W.Z. Zhu, S.C. Deevi, Mater. Res. Bull. 38 (2003) 957.
[3] K. Huang, P.Y. Hou, J.B. Goodenough, Solid State Ionics 129 (2000) 237.
[4] Z. Yang, K.S. Weil, D.M. Paxton, J.W. Stevenson, J. Electrochem. Soc. 150 (2003) A1188.
[5] H.G. Graham, H.H. Davis, J. Am. Ceram. Soc. 54 (1971) 89.
[6] K. Hilpert, D. Das, M. Miller, D.H. Peck, R. Weiβ, J. Electrochem. Soc. 143 (1996) 3642.
[7] S. Taniguchi, M. Kadowaki, H. Kawamura, T. Yasuo, Y. Akiyama, Y. Miyake, T. Saitoh, J. Power Sources 55 (1995) 73.
[8] S.P.S. Badwal, R. Deller, K. Foger, Y. Ramprakash, J.P. Zhang, Solid State Ionics 99 (1997) 297.
[9] S.C. Paulson, V.I. Birss, J. Electrochem. Soc. 151 (2004) A1961.
[10] S.P. Jiang, S. Zhang, Y.D. Zhen, J. Electrochem. Soc. 153 (2006) A127.
[11] S.P. Jiang, J.P. Zhang, K. Foger, J. Electrochem. Soc. 147 (2000) 3195.
[12] S.P. Jiang, J.P. Zhang, L. Apateanu, K. Foger, J. Electrochem. Soc. 147 (2000) 4013.
[13] S.P. Jiang, S. Zhang, Y.D. Zhen, J. Mater. Res. 20 (2005) 747.
[14] S.P. Jiang, J.P. Zhang, X.G. Zheng, J. Eur. Ceram. Soc. 22 (2002) 361.
[15] E. Konysheva, H. Penkalla, E. Wessel, J. Mertens, U. Seeling, L. Singheiser, K. Hilpert, J. Electrochem. Soc. 153 (2006) A765.
[16] W. Qu, L. Jian, J.M. Hill, D.G. Ivey, J. Power Sources 153 (2006) 114.
[17] Y.D. Zhen, A.I.Y. Tok, S.P. Jiang, F. Boey, J. Power Sources 170 (2007) 61.
[18] Y.D. Zhen, S.P. Jiang, A.I.Y. Tok, ECS Trans. 7 (1) (2007) 263.
[19] T. Komatsu, H. Arai, R. Chiba, K. Nozawa, M. Arakawa, K. Sato, Electrochem. Solid-State Lett. 9 (2006) A9.
[20] S.B. Adler, J.A. Lane, B.C. Steele, J. Electrochem. Soc. 143 (1996) 3554.
[21] M. Liu, Z. Wu, Solid State Ionics 107 (1998) 105.
[22] A. Esquirol, N.P. Brandon, J.A. Kilner, M. Mogensen, J. Electrochem. Soc. 151 (2004) A1847.
[23] M.R. James, R. Cecile, K. Romesh, J. Electrochem. Soc. 150 (2003) A1518.
[24] C. Xia, W. Rauch, M. Liu, Solid State Ionics 149 (2002) 11.
[25] Z. Shao, S.M. Haile, Nature 431 (2004) 170.
[26] M. Pechini, US Patent No. 3,330,697, 11 July 1967.
[27] S.P. Jiang, Solid State Ionics 146 (2002) 1.
[28] K. Fujita, T. Hashimoto, K. Ogasawara, H. Kameda, Y. Matsuzaki, T. Sakurai, J. Power Sources 131 (2004) 270.
[29] R.D. Shannon, Acta Cryst. A 32 (1976) 751.
[30] S.P. Jiang, L. Liu, K.P. Ong, P. Wu, J. Li, J. Pu, J. Power Sources 176 (2008) 82.